ARTICLE

TRPV6 Variants Interfere with Maternal-Fetal Calcium Transport through the Placenta and Cause Transient Neonatal Hyperparathyroidism

Yoshiro Suzuki,[1,2,14] David Chitayat,[3,4,14,*] Hirotake Sawada,[5] Matthew A. Deardorff,[6] Heather M. McLaughlin,[7] Amber Begtrup,[7] Kathryn Millar,[3] Jennifer Harrington,[8] Karen Chong,[3] Maian Roifman,[3] Katheryn Grand,[6] Makoto Tominaga,[1,2] Fumio Takada,[9,10] Shirley Shuster,[3] Megumi Obara,[5] Hiroshi Mutoh,[11] Reiko Kushima,[12] and Gen Nishimura[13]

Transient neonatal hyperparathyroidism (TNHP) is etiologically a heterogeneous condition. One of the etiologies is an insufficient maternal-fetal calcium transport through the placenta. We report six subjects with homozygous and/or compound-heterozygous mutations in the gene encoding the transient receptor potential cation channel, subfamily V, member 6 (*TRPV6*), an epithelial Ca^{2+}-selective channel associated with this condition. Exome sequencing on two neonates with skeletal findings consistent with neonatal hyperparathyroidism identified homozygous frameshift mutations before the first transmembrane domain in a subject born to first-cousins parents of Pakistani descent as well as compound-heterozygous mutations (a combination of a frameshift mutation and an intronic mutation that alters mRNA splicing) in an individual born to a non-consanguineous couple of African descent. Subsequently, targeted mutation analysis of *TRPV6* performed on four other individuals (born to non-consanguineous Japanese parents) with similar X-rays findings identified compound-heterozygous mutations. The skeletal findings improved or resolved in most subjects during the first few months of life. We identified three missense variants (at the outer edges of the second and third transmembrane domains) that alter the localization of the TRPV6: one recurrent variant at the S2-S3 loop and two recurrent variants (in the fourth ankyrin repeat domain) that impair TRPV6 stability. Compound heterozygous loss-of-function mutations for the pathogenic frameshift allele and the allele with an intronic c.607+5G>A mutation resulted in the most severe phenotype. These results suggest that TNHP is an autosomal-recessive disease caused by *TRPV6* mutations that affect maternal-fetal calcium transport.

Introduction

Calcium (Ca^{2+}) is essential for many physiological functions in most of the cells in our body, and the blood $Ca2^{+}$ level (the amount of Ca^{2+} in the blood) is strictly maintained both pre- and postnatally. Prenatally, in additional to proper Ca^{2+} concentration for optimal cellular function, the fetus requires additional Ca^{2+} for skeletal formation and mineralization. Blood Ca^{2+} level has been reported to be higher in the fetus than in the mother,[1] indicating that there is active Ca^{2+} transport from the mother to fetus during pregnancy.

For active transplacental maternal-fetal transport of calcium, three placental trophoblast molecular processes play major roles: (1) apical Ca^{2+} entry through Ca^{2+} channels via an electrochemical gradient, (2) binding of Ca^{2+} to calbindin D to prevent increase of free Ca^{2+} concentration, and (3) basolateral Ca^{2+} extrusion, which occurs mainly via Ca^{2+}ATPase. It has been suggested that an epithelial Ca^{2+}-selective channel called TRPV6 (the transient receptor potential cation channel, subfamily V, member 6), calbindin D_{9K}, and the plasma membrane Ca^{2+} ATPase are molecular candidates for each of these processes, respectively. Despite strong data implicating these candidates in the process of transplacental transport of calcium, they have yet to be implicated in human disease.

Using exome sequencing, we have identified recessive *TRPV6* (MIM: 606680) mutations that cause transient neonatal hyperparathyroidism (TNHP) with skeletal abnormalities. These findings demonstrate a clear association between TNHP and *TRPV6* mutations. Although TNHP has been well recognized and its transient occurrence raised the possibility that it is the result of insufficient maternal-fetal Ca^{2+} transport, this work demonstrates that the molecular etiology of the condition is due to a TRP channel disease.

[1]Division of Cell Signaling, Okazaki Institute for Integrative Bioscience (National Institute for Physiological Sciences), National Institutes of Natural Sciences, Okazaki 444-8787, Japan; [2]Department of Physiological Sciences, SOKENDAI (The Graduate University for Advanced Studies), Okazaki 444-8787, Japan; [3]The Prenatal Diagnosis and Medical Genetics Program, Department of Obstetrics and Gynecology, Mount Sinai Hospital, University of Toronto, Toronto, ON M5G 1Z5, Canada; [4]Division of Clinical Genetics and Metabolism, Department of Pediatrics, The Hospital for Sick Children, University of Toronto, Toronto, ON M5G 1X8, Canada; [5]Division of Pediatrics, Department of Developmental and Urological-Reproductive Medicine, Faculty of Medicine, University of Miyazaki, Miyazaki 889-1692, Japan; [6]Division of Human Genetics, Children's Hospital of Philadelphia, Philadelphia, PA 19104, USA; [7]GeneDx, Gaithersburg, MD 20877, USA; [8]Division of Endocrinology and Metabolism, Department of Pediatrics, The Hospital for Sick Children, University of Toronto, Toronto, ON M5G 1X8, Canada; [9]Department of Medical Genetics and Genomics, Graduate School of Medical Sciences, Kitasato University, Kanagawa 252-0375, Japan; [10]Division of Genetics and Genomics, Center for Clinical Genetics and Genomics, Kitasato University Hospital, Kanagawa 252-0374, Japan; [11]Department of Neonatology, Tokyo Metropolitan Children's Medical Center, Tokyo 183-8561, Japan; [12]Department of Neonatology, Tokyo Metropolitan Bokutoh Hospital, Tokyo 130-8575, Japan; [13]Intractable Disease Center, Saitama Medical University Hospital, Saitama 350-1298, Japan
[14]These authors contributed equally to this work
*Correspondence: david.chitayat@sinaihealthsystem.ca
https://doi.org/10.1016/j.ajhg.2018.04.006.

Material and Methods

This study was approved by the Mount Sinai Hospital's research ethics board (MSH REB 17-0172-C) after each of the parents gave informed consent.

Exome sequencing was performed on genomic DNA extracted from whole blood from the affected children and their parents. Subjects 1 and 6 had clinical exome sequencing performed at GeneDx with exon targets isolated by capture with the Agilent SureSelect Human All Exon V4 kit or the Clinical Research Exome kit (Agilent Technologies, Santa Clara, CA). The sequencing technology and variant-interpretation protocol has been previously described.[2] The general assertion criteria for variant classification are publicly available on the GeneDx ClinVar submission page (Web Resources).

Sanger Sequencing

Validation of the mutation candidates detected by WES and the mutation analysis of the *TRPV6* (GenBank: NM_018646.5 and NT_007933.16) in subjects 2–5 was performed by Sanger sequencing on the subjects and their parents. PCR primers and conditions are available upon request.

Construction of TRPV6 Plasmid with Disease Mutations

The full-length human *TRPV6* cDNA in pNWP vector was provided by Dr. Matthias A. Hediger (University of Bern, Switzerland) (GenBank: Af365927).[3] *TRPV6* cDNA was amplified with primers (5′-GCCGCCACCACGGGACCTCTACAGGGA GAC-3′ and 5′-TAAGCGGCCGCTCAGATCTGATATTCCCAG-3′) through the use of PrimeSTAR Max DNA polymerase (Takara, Japan) and with the full-length human TRPV6 cDNA in pNWP vector as a template. PCR reaction was as follows: 35 cycles of 98°C for 10 s, 55°C for 5 s, and 72°C for 20 s. Kozak sequence was added in this reaction as described previously, just upstream of the non-AUG start site, which has been reported to be predominantly used as the translational start site of TRPV6 in human placenta.[4] The amplified fragments were treated with T4 polynucleotide kinase (Takara), purified by Nucleospin (Takara), and digested with Not I-HF (NEB, USA) and then ligated by Ligation high ver. 2 (Toyobo, Japan) with pcDNA3.1(+) (Life Technologies, USA) and pretreated with Eco*R*V-HF (NEB) and Not I-HF. The sequence of this construct was confirmed by sequencing (ABI PRISM3130xl, ABI, USA).

We carried out mutagenesis PCR using PrimeSTAR Max with the plasmid TRPV6 cDNA in pcDNA3.1(+) under the following condition except for c.52G>T (p.Ala18Ser): 30 cycles of 98°C for 10 s, 55°C for 15 s, and 72°C for 40 s. The primers for the mutagenesis are listed in the Supplemental Methods. For p.Ala18Ser, the PrimeSTAR system (TaKaRa, Japan) with Dpn I was used according to the manufacturer's instructions. For electrophysiology, these constructs were used without a Myc tag. For immunoblotting, the double-Myc (2Myc) tag was added to the above-mentioned plasmid. These mutations were confirmed by DNA sequencing. The channel function of the 2Myc-TRPV6 WT was confirmed by whole-cell patch-clamp recordings, which did not differ significantly from those of untagged WT TRPV6.

Cell Culture and Transfection

Human embryonic kidney-derived 293T (HEK293T) cells were maintained in DMEM with 10% heat-inactivated FBS, 100 units/mL penicillin and streptomycin, 2 mM L-glutamine, and 5% CO_2 at 37°C. Using Lipofectamine reagent (Life Technologies), we transfected HEK293T cells with the above-mentioned TRPV6 plasmid (1 μg) and pGL1 plasmid (0.1 μg). We identified transfected cells by GFP fluorescence.

Electrophysiology

Whole-cell patch-clamp recordings were performed as described previously[5] but with some modifications. Standard bath solution contained 143 mM NaCl, 5 mM KCl, 2 mM $MgCl_2$, 5 mM HEPES (pH 7.4 with NaOH), 10 mM glucose, and 1 mM $CaCl_2$. The divalent-cation-free (DVF) solution contained 148 mM NaCl, 5 mM KCl, 5 mM HEPES (pH 7.4 with NaOH), and 10 mM glucose. The *N*-Methyl-D-glucamine (NMDG) solution contained 149 mM NMDG, 2 mM $MgCl_2$, 5 mM HEPES (pH 7.4 with HCl), 10 mM glucose, and 1 mM $CaCl_2$. The calcium bath contained 105 mM NMDG, 2 mM $MgCl_2$, 5 mM HEPES (pH 7.4 with HCl), 10 mM glucose, and 30 mM $CaCl_2$. The pipette solution contained 100 mM Cs-aspartate, 40 mM CsCl, 1 mM $MgCl_2$, 10 mM EGTA, and 5 mM HEPES (pH 7.2 with CsOH). Osmolarity was 292 ± 5 mOsm/kg. Data were sampled at 10 kHz with an Axon 700B amplifier with pCLAMP software (Axon Instruments). Membrane potential was clamped at −60 mV. In ramp experiments, voltage ramp pulses from −150 mV to +100 mV (400 ms) were applied every 5 s. We calculated the current densities by dividing the peak amplitude of current at −60 mV by membrane capacitance. All experiments were performed at room temperature. For the c.1352G>A (p.Gly451Glu) variant, recordings were performed within 24 hr after transfection.

Plasma Membrane Protein Biotinylation

Biotinylation of plasma membrane proteins was performed as described previously, with some modifications.[6] *TRPV6* plasmid was transfected into HEK293T cells as described above and incubated for 28 hr. Cells were washed with PBS and incubated twice with 0.5 mg/mL EZ-Link NHS-LC-Biotin (Abcam #ab145611) in PBS for 10 min each in CO_2 incubator. Cells were washed with quenching buffer (100 mM glycine in PBS) and with PBS before being lysed in lysis buffer (1× TNE buffer [200 μl/35 mm dish] with 1% NP-40 and protease inhibitor cocktail [Complete, Roche]). Proteins (total lysate) were incubated with Streptavidin magnetic beads (Dynabeads MyOne Strept T1, Invitrogen) overnight at 4°C with rotation, according to the manufacturer's instructions. Beads were collected by magnet, washed with lysis buffer three times, and denatured at 95°C for 5 min with 80 μLl of 1× SDS sample buffer and 0.1 M DTT. Samples (plasma membrane) were kept at −20°C until use.

Immunoblotting

SDS-PAGE was performed with the above protein samples (total lysate or plasma membrane) in 6% polyacrylamide gel (Biorad) and transferred into a polyvinylidene fluoride membrane (Immobilon-P, Millipore). The membrane was incubated overnight at 4°C with 3% BSA in PBS with 0.1% Tween-20 (PBST) for blocking and then incubated with mouse anti-c-*myc* antibody (Sigma #M5546, 1/500 dilution in 3% BSA in PBST) or rabbit anti-TRPV6 antibody (Alomone #ACC-036, 1/500) for 2 hr at room temperature. After being washed three times with PBST, the membrane was treated with anti-mouse IgG-HRP (CST, 1/3,000 dilution) for 30 min at room temperature. After these three washes, signals were visualized with an ECL prime kit (Amersham). The mouse anti-c-*myc* antibody identified a band of approximately

80 kDa at the same position as that of the anti-TRPV6 antibody (data not shown).

Measurement of Intracellular Ca^{2+} Concentration

HEK293T cells were transfected with plasmid containing WT *TRPV6* or the above-mentioned variants (1 μg) and pCMV-DsRed-Express plasmid (0.1 μg, Clontech). After 24 hr, cells were incubated with the fluorescent Ca^{2+} indicator Fura-2 (5 μM, Fura-2-acetoxymethyl ester, Life Technologies) in DMEM at 37°C for 1 hr. Cytosolic Ca^{2+} concentration was measured in a steady state with a standard bath solution (143 mM NaCl, 5 mM KCl, 2 mM $CaCl_2$, 2 mM $MgCl_2$, 10 mM glucose, and 5 mM HEPES [pH 7.4]). Ratiometric imaging was performed at 340 nm and 380 nm, and the emitted light was read at 510 nm with a CCD camera (CoolSnap ES, Photometrics, Roper Scientific). The ratio of F340/380 was calculated by IP-Lab software (Scanalysis), and data from Ds-Red-positive cells were acquired with ImageJ software (Web Resources).

Minigene Assay

A minigene construct of *TRPV6* (Figure S3A) was amplified with primers (5′-CAGACTGCACTGCACATCGCTG-3′ and 5′-TTACT CCCGCTTCTTGGTGGTGATG-3′) via Phusion DNA polymerase (NEB, USA) with genomic DNA from a normal individual as a template. The PCR reaction was carried out as follows: 98°C for 30 s, 40 cycles of 98°C for 10 s and 72°C for 1 min, and 72°C for 2 min. A stop codon was added at the end of exon 7 (Figure S3A). Amplified fragments were treated with T4 polynucleotide kinase (Takara, Japan), ligated by T4 ligase (ToYoBo, Japan) with pcDNA3.1 (+) (Life Technologies, USA), and pretreated with Eco*R*V-HF (NEB, USA) and CIP (Takara, Japan). The sequence was confirmed by DNA sequencing. To introduce c.607+5G>A mutation, mutagenesis was carried out with HiFi DNA assembly system (NEB, USA).

The minigene construct with the mutation of individual 6 was transiently transfected into HEK293T cells as described above. After 24 hr, RNA was extracted by Sepasol RNA I kit (Nacalai, Japan). First-strand cDNA was synthesized by Superscript III (Thermo Fisher, USA) with oligo $(dT)_{20}$. PCR was carried out with primers indicated as arrowheads in Figure S3A (5′-CTGCAACCTCATCTACTTTG-3′ and 5′-TGCATCAGGTGCTGAAACAT-3′). The PCR reaction was carried out as follows: 94°C for 2 min, then 25 cycles of 94°C for 30 s, 45°C for 30 s, and 72°C for 30 s. PCR fragments were visualized by agarose gel electrophoresis. Sequences of these PCR fragments were analyzed after the fragments were subcloned into the pGEM-Teasy vector system (Promega, USA).

Statistical Analysis

Statistical analysis was performed with an unpaired t test or Mann-Whitney rank-sum test. Differences with p values of less than 0.05 were considered significant.

Results

A detailed description of the clinical findings of the six individuals is available in the Supplemental Note. Subject 1 (A II-1 in Figure 1), subject 2 (B II-1 in Figure 1), subject 3 (C II-2 in Figure 1), subject 4 (D II-3 in Figure 1), and subject 5 (E II-3 in Figure 1) had prenatal history of skeletal abnormalities detected in the third trimester of pregnancy. It is not clear whether a third-trimester ultrasound was done on subject 6 (F II-1 in Figure 1) (Table 1 and Supplemental Note). All subjects presented with elevated serum PTH and alkaline phosphatase activity. Ionized calcium that was measured by potentiometric ion-selective electrode was normal in subjects 1–3 but low in subjects 4 and 5 (Table 2) (ionized calcium was not measured in subject 6 because the baby was initially felt to have osteogenesis imperfecta). PTH levels measured over many time points for subjects 2–5 demonstrated a pattern of decline with age, as shown in Figure S2. X-ray findings at birth for most subjects resembled the changes seen in neonatal hyperparathyroidism. Subjects 1–5 had complete recovery by age 2 years, whereas subject 6 had hydrocephalus and chest expanders placed at 7 months of age. However, her skeletal abnormalities also gradually improved (Figure 2 and Figure S1). Subjects 1–5 had developmental milestones within the normal range, and subject 6 was delayed most likely because of cerebral complications (Supplemental Note).

Exome sequencing was performed on two subjects with neonatal bone disease that overlapped a clinical picture of TNHP or osteogenesis imperfecta. This approach identified a homozygous variant (GenBank: NM_018646.5; c.530_533dup [p.Arg179CysfsTer18]) in *TRPV6* in subject 1 (Figures 1A and 3) and compound-heterozygous *TRPV6* potential loss-of-function alleles: a c.607+5G>A splice-site allele inherited from the mother and a c.978_979del (p.Asp328*) frameshift allele inherited from the father (Figures 1F and 3) in subject 6.

Subsequent Sanger sequencing performed on subjects 2–5, who had TNHP, identified compound-heterozygous missense mutations in *TRPV6*: c.635G>A (p.Cys212Tyr) and c.1282G>A (p.Gly428Arg) in subject 2, c.668T>C (p.Ile223Thr) and c.1274G>A (p.Arg425Gln) in subject 3, c.1352G>A (p.Gly451Glu) and c.1447C>T (p.Arg483Trp) in subject 4, and c.1274G>A (p.Arg425Gln) and c.1352G>A (p.Gly451Glu) in subject 5 (Figures 1B–1E). These mutations were absent from public databases (1000 Genomes Project, 6,503 exomes from the Exome Sequencing Project [ESP6500SI], and Exome Aggregation Consortium [ExAC] Browser v0.3). Sanger sequencing of the parents demonstrated segregation of the mutations with the TNHP phenotype (Figure 1).

In these TNHP subjects, three variants (p.Arg425Gln, p.Gly428Arg, and p.Arg483Trp) were found in the transmembrane domains (S2 and S3), two variants (p.Cys212Tyr and p.Ile223Thr) in the ankyrin repeat domain 4, and one variant (p.Gly451Glu) in the intracellular S2-S3 loop (Figure 3A). To assess the functional significance of these variants, we introduced them into *TRPV6* cDNA construct and transfected them into HEK293T cells before taking whole-cell patch-clamp recordings. Figure 3B shows a representative time trace of mock-transfected cells, WT cells, or p.Arg425Gln-expressing HEK293T cells with alterations of extracellular solution while the potential was held at −60 mV. In WT-expressing cells, when DVF solution was superfused, monovalent cation

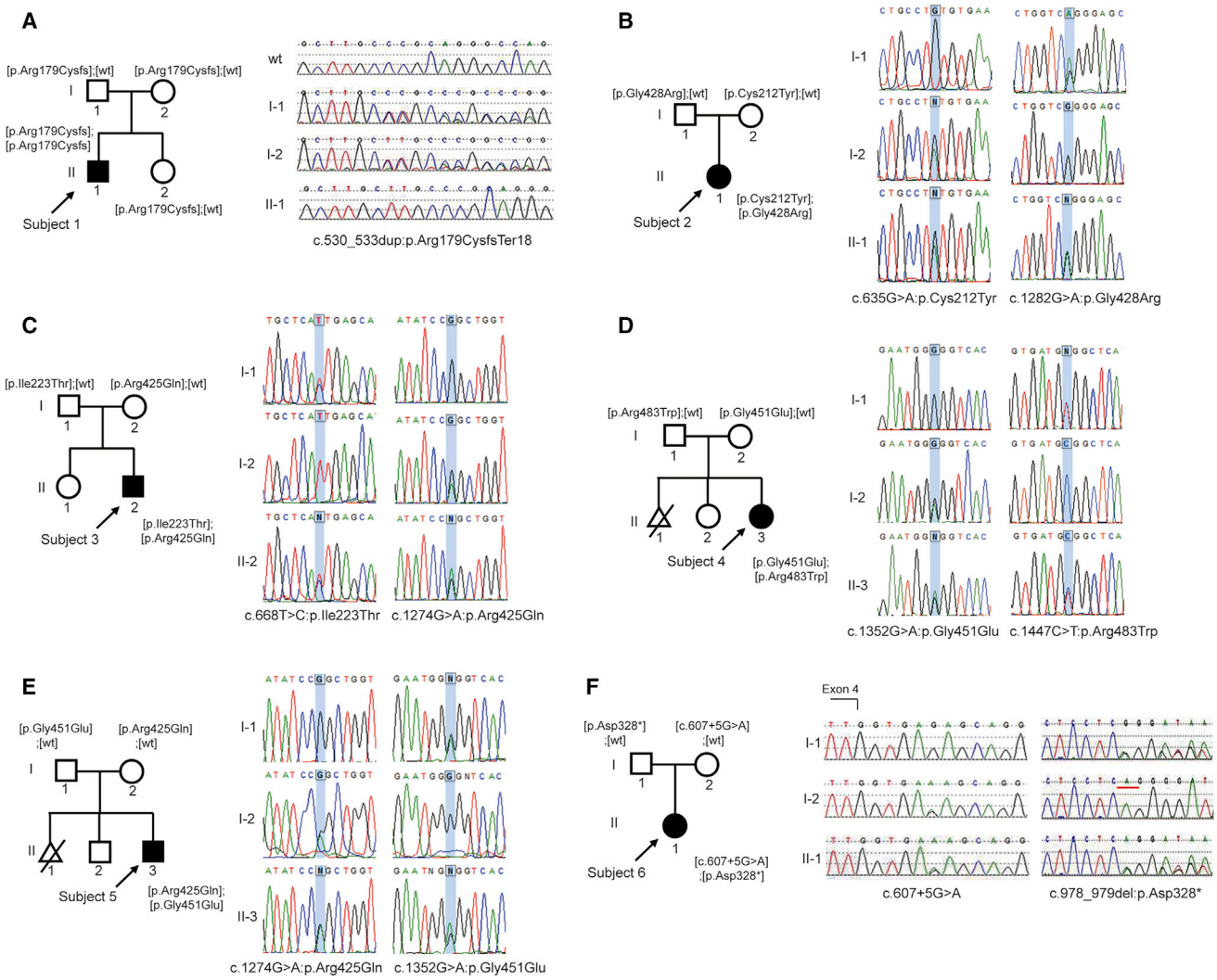

Figure 1. Pedigrees of the Six Families with TNHP and Sanger Sequencing Confirming the Identified Mutations in *TRPV6* that Show Complete Cosegregation with Phenotype

(A) Analysis showing that the parents (I-1 and I-2) are heterozygote and the affected child (II-1) is homozygote for the familial gene mutation.

(B) Analysis showing that the parents (I-1 and I-2) are heterozygote and the affected child (II-1) is compound heterozygote for the gene mutations.

(C) Analysis showing that the parents (I-1 and I-2) are heterozygote and the affected child (II-2) is compound heterozygote for the gene mutations.

(D) Analysis showing that the parents (I-1 and I-2) are heterozygote and the affected child (II-3) is compound heterozygote for the gene mutations.

(E) Analysis showing that the parents (I-1 and I-2) are heterozygote and the affected child (II-3) is compound heterozygote for the gene mutations.

(F) Analysis showing that the parents (I-1 and I-2) are heterozygote and the affected child (II-1) is compound heterozygote for the gene mutations.

currents were observed as shown in previous reports.[7,8] These currents had an inwardly rectifying current-voltage relationship (data not shown). When all extracellular monovalent cations were substituted with $NMDG^+$, the inward currents were abolished, indicating that the monovalent cations were the charge carriers for the inward currents in DVF solution. When the solution was changed to 30 mM Ca^{2+}, large currents with time-dependent inactivation kinetics were observed as previously reported (n = 8). These data are consistent with a Ca^{2+} current, given that Ca^{2+} was the only charge carrier. However, these inward currents were not observed in p.Arg425Gln-expressing cells (n = 6). This phenomenon was also seen for p.Cys212Tyr, p.Gly428Arg, and p.Arg483Trp variants (Figures 3B and 3C). In contrast, p.Ile223Thr and p.Gly451Glu variants exhibited calcium and monovalent cation currents that were similar to WT *TRPV6*. We noted no significant difference between WT and p.Ile223Thr or p.Gly451Glu variants with respect to current amplitude or intracellular Ca^{2+} concentration ($[Ca^{2+}]_i$)-dependent

Table 1. Pre- and Postnatal Clinical Findings in Six Subjects with TRPV6 Variants

	Ethnic Background	Maternal/Paternal Age (Years)	Prenatal Ultrasound Findings	GA at Delivery (Weeks)	Birth Weight/Length/OFC (Percentile)	PTH (pmol/L; Normal = 1–6.9)	Postnatal Respiratory Difficulties	CMA or Chromosome Analysis	Age at Complete Resolution of Skeletal Abnormalities
Subject 1	Pakistani, consanguineous	23/27	at 31.3 weeks: right renal agenesis, enlarged echogenic left kidney, short and bell-shaped chest, short ribs, polyhydramnios	39.5	$10^{th}/90^{th}/50^{th}$	9.7	yes	normal male	1.5 years
Subject 2	Japanese, non-consanguineous	35/36	at 35 weeks: polyhydramnios, short long bones with femoral length of 53.4 mm (−4.5 SD)	38	$<3^{rd}/3^{rd}/50^{th}–90^{th}$	239.7	yes	46, XX	1.5 years
Subject 3	Japanese, non-consanguineous	32/32	at 28 weeks: polyhydramnios; at 34 weeks: short and bowed femurs	39.1	$3^{rd}/<3^{rd}/50^{th}–90^{th}$	13.8 (at 1 month)	yes	46, XY	2 years
Subject 4	Japanese, non-consanguineous	38/?	in the third trimester: thoracic narrowing with rib deformities	38	$3^{rd}/<3^{rd}/50^{th}–90^{th}$	154.8	yes	46, XX	2 years
Subject 5	Japanese, non-consanguineous	34/42	at 20 weeks: no abnormalities detected	34	$87^{th}/66^{th}/97^{th}$	28.73	yes	46, XY	1 year
Subject 6	Barbadian and Jamaican	29/39	reportedly normal; not clear whether third-trimester ultrasound was done	38	$<3^{rd}/3^{rd}/90^{th}$	22.76	yes	female; 2–3 kb 16p13.3 deletion	still abnormal but substantially improved

Abbreviations are as follows: Wt, weight; GA, gestational age; OFC, head circumference; and CMA, chromosome microarray analysis.

inactivation in our whole-cell patch-clamp recordings, although the mean peak amplitude was smaller in p.Ile223Thr than in WT cells. In addition, there was no significant difference in c.52G>T (p.Ala18Ser) polymorphism cells compared to in WT cells (Figure 3C).

Next we focused on the mechanism by which these variants failed to show membrane currents in patch-clamp recordings. We hypothesized that the variants caused a defect in plasma-membrane localization. Therefore, we analyzed plasma-membrane protein quantities by using a biotinylation assay. Our results demonstrated abnormal localization of the p.Arg425Gln, p.Gly428Arg, and p.Arg483Trp variants (Figures 3D and 3E) because they were deficient in reaching the plasma membrane. Interestingly, although we could observe Ca^{2+} currents in p.Gly451Glu variants 24 hr after transfection, there was almost no detectable TRPV6 both in plasma membrane or total cellular lysate 28 hr after transfection (Figures 3D and 3E). Furthermore, most of the transfected cells at 28 hr were round and detached from the culture dish, suggesting that the p.Gly451Glu variant results in cell death as a result of the Ca^{2+} overload, as previously reported in TRPV5 variants that impaired $[Ca^{2+}]_i$-dependent inactivation.[9] Of note, these previously reported TRPV5 residues (mouse Trpv5 p.Leu409Val, p.Val411Ala, and p.Thr412Ser), are next to human TRPV6 p.Gly451Glu (p.Gly410 in mouse) and are important for the $[Ca^{2+}]_i$-dependent inactivation.[10] The p.Gly451Glu variant protein was detectable when the incubation for transfection was shorter (24 hr) (Figure 3F). Moreover, the amount of p.Gly451Glu increased when 2 μM ruthenium red, a broad TRP channel blocker, was added into the medium after transfection (Figure 3F). We thus hypothesized that even in a steady state, the $[Ca^{2+}]_i$ was higher in p.Gly451Glu-expressing HEK293T cells than in WT cells. This was confirmed by Fura-2 imaging, which showed that in a steady state, $[Ca^{2+}]_i$ was significantly higher in a p.Gly451Glu variant than in the WT (Figure 3G). These results strongly suggest that $[Ca^{2+}]_i$-dependent inactivation was impaired in p.Gly451Glu variants and led to cell death as a result of Ca^{2+} overload.

Subject 6 also had compound-heterozygous mutations with a presumed loss-of-function frameshift mutation, c.978_979del (p.Asp328*), and a *trans*-splice site mutation of intron 4, c.607+5G>A (Figure S3A). In general, the +1 and +2 positions are 100% conserved, and the +5 position with approximately 85% conservation in humans, is next-most stringent. To confirm that the alteration of this +5 position was pathogenic, we performed minigene assays with or without a c.607+5G>A mutation (Figure S3A), which we introduced into the pcDNA3.1 vector and transfected into HEK293T cells. After 24 hr, we performed RT-PCR with the primers indicated by arrowheads in Figure S3A. Although we anticipated exon-skipping (which would produce a 216 bp band), a longer band was observed (Figure S3B). We confirmed that a short intronic sequence of 41 bp was

Table 2. The Newborns' Blood Test Results

	Ionized Calcium (mmol/L)	Phosphorus (mmol/L)	Alkaline Phosphatase (U/L)	iPTH (pmol/L)	1,25-Dihydroxyvitamin D (pmol/L)	25OH Vitamin D (nmol/L)	Creatinine (μmol/L)
Subject 1	1.27	1.45	871[a]	9.7[a]	392[a] (1 month)	99	21[a]
Subject 2	1.14	1.51	576[a]	239.7[a]	95.7	27.5	23.0[a]
Subject 3	1.20	1.20	130 (1 month)	13.8[a] (1 month)	NA	NA	42.4
Subject 4	0.87[a]	1.87	NA	154.8[a]	NA	15.0[a]	NA
Subject 5	0.92[a]	2.23	905[a]	28.7[a]	NA	20.2	53.0
Subject 6	NA	1.55	815[a]	22.76[a]	84	26.4	NA
Normal range in neonates	1.1–1.3	1.6–2.6	28–300	1.3–6.8	31–151	75–200	27–88
Normal range in adults	1.1–1.35	0.8–1.45	115–359	1.1–6.9	48–155	17–102	58.3–94.6 (males), 39.8–71.6 (females)

Abbreviations are as follows: iPTH, intact parathyroid hormone; and NA, not available.
[a]The value is out of the normal range for both neonates and adults.

inserted into *TRPV6* mRNA and that this insertion led to a frameshift (Figure S3D). It seemed that the incorrect splicing site was a normally unused cryptic splice site (Figure S3C). These results suggest that c.607+5G>A is a severe loss-of-function mutation that affects the majority of mRNAs.

Discussion

Maternal-fetal transport of calcium is of utmost importance for fetal bone formation and mineralization, cell function, blood coagulation, and neuromuscular activity.[11] During pregnancy, 25–30 g of calcium is transported to the fetus from the mother through the placenta,[12,13] and about 80% of the calcium is transferred during the third trimester. Thus, defective transplacental transport of calcium would not expected to result in fetal bone changes during the second trimester, a finding consistent with these individuals who showed no abnormalities on second-trimester detailed ultrasound. Because calcium is being transported from the mother to the fetus against a concentration gradient,[14] a transport mechanism is needed to provide the fetus with a steady supplementation of calcium.

Neonatal hyperparathyroidism can be primary and is in most of these subject caused by homozygous inactivating *CASR* (MIM: 601199) mutations[15] as well as by inactivating mutations in *CASR*-associated G protein alpha 11 (*GNA11* [MIM: 139313]) and in the adaptor-related protein complex 2 sigma 1 subunit (*AP2S1* [MIM: 602242]).[16–19] These mutations reduce the sensitivity of the CaSR to extracellular calcium, causing increased secretion of PTH and decreased renal excretion of calcium.

Neonatal hyperparathyroidism can also be secondary and was reported to be associated with compound-heterozygous mutation in *SLC12A1* (MIM: 600839), encoding the sodium-potassium-chloride cotransporter-2 (NKCC2). Mutations in this gene are known to be associated with antenatal Bartter syndrome. Li et al. raised the possibility that the elevated levels of prostaglandin E2 identified in antenatal Bartter syndrome cause an increased PTH secretion, causing elevated $1,25(OH)_2D$ levels and, in some cases, hypercalcemia.[20]

Secondary neonatal hyperparathyroidism was reported in association with mucolipidosis type II (ML II), caused by homozygous and/or compound-heterozygous mutations in *GNPTAB* (MIM: 252500).[21] Unger et al. suggested that the mechanism for this association is that the enzyme-targeting defect of ML II interferes with transplacental calcium transport and that this interference leads to fetal calcium deficiency and activation of the parathyroid response to maintain normal extracellular calcium concentration. Another rare reported cause of secondary TNHP is maternal pseudohypoparathyriodism, thought to be caused by transfer of PTH to the fetus through the placenta.[22]

We report here a cause for secondary hyperparathyroidism—deficient maternal-fetal transfer of calcium through the placenta caused by a homozygous and/or compound-heterozygous variant in *TRPV6*. The transient receptor potential channel type 6 (encoded by *TRPV6*) plays a major role in the active calcium (Ca^{2+}) transport mechanism in many tissues, including the placenta and the uterus, suggesting a role in the establishment and maintenance of pregnancy.[23] The functional TRPV6 channel comprises four identical subunits, each with six transmembrane segments (S1–S6), to form an inwardly rectifying Ca^{2+}-selective ion channel.

TRPV6 was mapped to chromosome 7q33−q34, spans 15 exons, and extends over a region of about 15.7 kb. Although *TRPV6* expression has been found to be upregulated in prostate and breast cancer and has also been found to play a role in the intestinal Ca^{2+} absorption from food[24,25] and in the Ca^{2+} uptake by the epididymal epithelium,[26–28] no specific human disease has been found to be associated with *TRPV6*.[29,30]

Figure 2. Subjects' Radiological Findings
(A–C) Subject 1 in the neonatal period: the ribs are thin, deformed, and fractured. The thorax is narrow. The long bones show metaphyseal constriction (arrowheads) and diaphyseal tunneling (arrows) as a result of subperiosteal resorption. The femora are mildly bowed.
(D–E) Subject 1 at 2 years of age: The skeletal changes have normalized.
(F–H) Subject 4 as a neonate (F), at 2 months of age(G), and at 6 months of age (H). Rib deformities and femoral bowing (F) completely resolved during infancy (G&H).
(I–J) Subject 4, fetal CT: Note rib deformities and femoral bowing.

In this work, we demonstrate that biallelic pathogenic variants in *TRPV6* cause TNHP with bone abnormalities in six individuals. This disease is most likely caused by insufficient maternal-fetal Ca^{2+} transport through the placenta to sustain fetal bone mineralization. Both fetal CT (computed tomography) and ultrasound findings indicate an impaired Ca^{2+} transport through the placenta (Figures 2I and 2J), elevated intact PTH level (seen in all our subjects), and hypocalcemia, seen in the neonatal period (days 0–2). Furthermore, individuals 4 and 5 clearly demonstrate a negative Ca^{2+} balance in the fetuses, consistent with a significant decrease in maternal-fetal Ca^{2+} transport. These findings recapitulate the phenotypes identified in systemic *Trpv6*-knockout mice.[31] These mice exhibit fetal hypocalcemia with normal Mg^{2+} levels and a significant decrease in bone mineral weight along with a substantial decrease in the radioactive Ca^{2+} [$^{45}Ca^{2+}$] transport from the mother to the fetus.

Each of our subjects had at least one complete loss-of-function mutation, such as a nonsense or frameshift mutation or a mutation that fully abrogated localization of TRPV6 proteins to the plasma membrane.[32] For all subjects with compound-heterozygous mutations, the second allele disrupted RNA splicing, altered protein localization (p.Arg425Gln, p.Gly428Arg, or p.Arg483Trp), or impaired protein stability (p.Cys212Tyr or p.Ile223Thr). The net effect for each subject was an absent or markedly reduced functional TRPV6 channel, thus reducing the maternal-fetal Ca^{2+} transport. We speculate that this increased Ca^{2+} demand further upregulates the maternal-fetal Ca^{2+} transport system and the expression of *TRPV6* mRNA and that, in some instances, this upregulation leads to the overexpression of an abnormal allele.

Interestingly, the p.Gly451Glu variant was found in two of our six subjects. When expressed in HEK293T cells, the p.Gly451Glu variant exhibited significantly higher $[Ca^{2+}]_i$ in a steady state than the WT and, most likely because of the intracellular Ca^{2+} overload, demonstrated increased cell death. We hypothesize that this variant represents a toxic allele that could be exacerbated by this upregulation of its expression. The $[Ca^{2+}]_i$-dependent inactivation is an essential characteristic for avoiding Ca^{2+} overload in most Ca^{2+}-permeable channels. It has been reported that TRPV6 possesses an intrinsic as well as a Ca^{2+}-calmodulin-dependent inactivation mechanism.[10,33–35] Several protein regions, including the N terminus and C terminus, have been reported to be important for the Ca^{2+}-calmodulin-dependent inactivation in their role as calmodulin binding sites. Moreover, although the detailed molecular mechanism is still unknown, Nilius et al. showed that three amino acid residues next to Gly451 were critical for the inactivation mechanism, which was likely to be channel-intrinsic.[10]

In comparison, the p.Cys212Tyr and p.Ile223Thr variants lie in the fourth ankyrin repeat domain. In these variants, immunoblot analysis and patch-clamp recordings indicated a decrease in functional in the plasma membrane, suggesting that these are partial loss-of-function variants. This effect is also seen for the c.607+5G>A

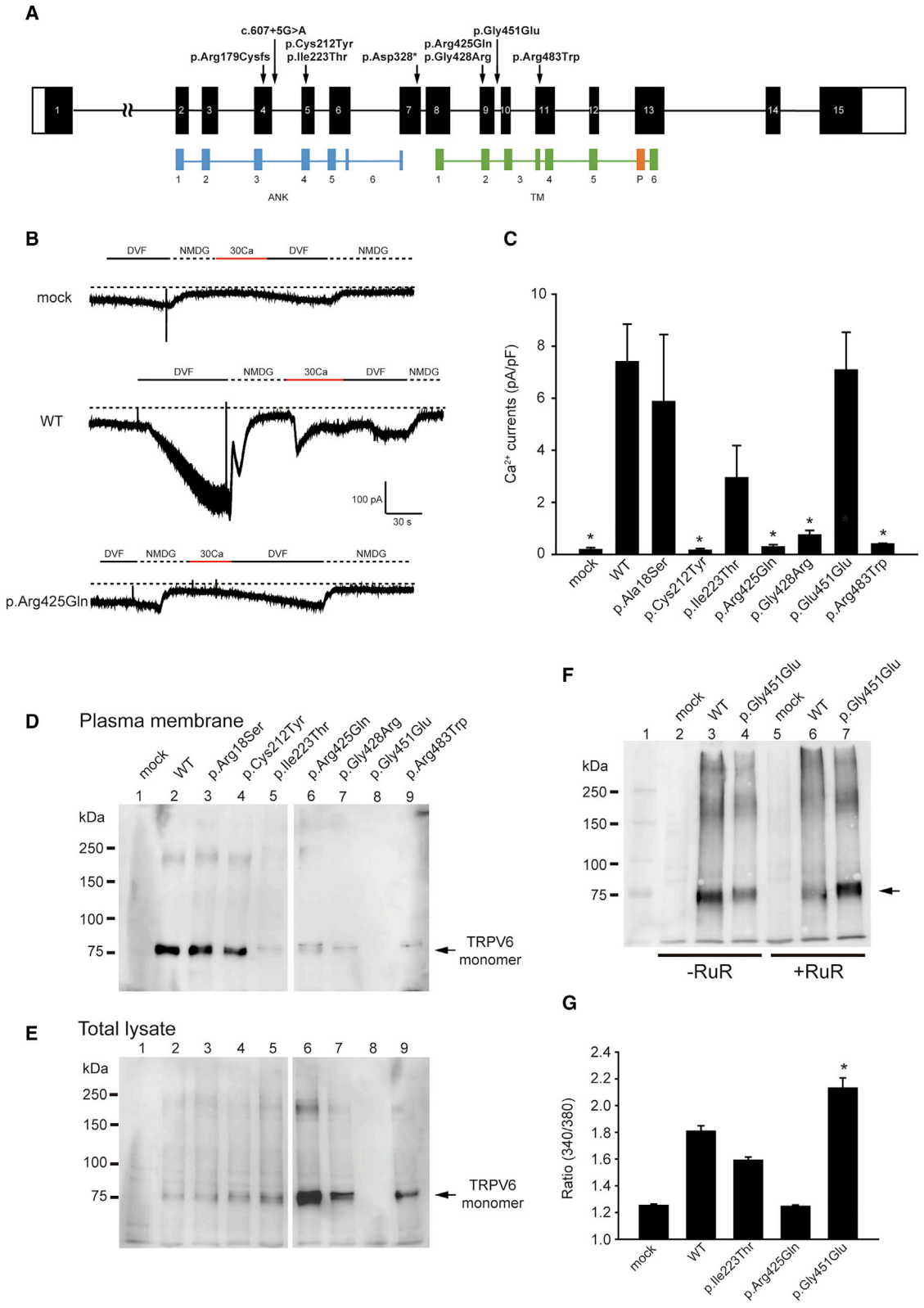

Figure 3. Functional Analysis of TRPV6 Variants

(A) Overview of the TRPV6 variants in six TNHP subjects. Two nonsense variants (p.Arg179CysfsTer18 and p.Asp328*) are suggested to result in complete loss of function. One mutation in intron 4 (c.607+5G>A) is predicted to affect mRNA splicing, resulting in a partial generation of a frameshift mutation. Three missense variants (p.Arg425Gln, p.Gly428Arg, and p.Arg483Trp) were found in the S2 and S3 transmembrane domains, two (p.Cys212Tyr and p.Ile223Thr) in the fourth ankyrin repeat domain (ANK4), and one (p.Gly451Glu) in the intracellular S2-S3 loop.

(legend continued on next page)

mutation, which severely affects mRNA splicing. Although it is still possible that these variants partially affect the localization to the plasma membrane, we suspect that the resulting proteins, if any, are recognized as abnormal and are degraded by the ubiquitin-proteasome pathway or other quality-control mechanisms, given that the ankyrin repeats have been reported to be critical for protein folding and the sites and characteristics of these residues are probably important for the structure of TRPV6.[32,36]

These observations raise interesting possibilities for potential therapeutic intervention. Small molecular chaperones such as those used for the treatment of the dysfunctional CFTR Cl^- channel in CF subjects could improve the conformation of TRPV6 variants and could be beneficial prenatally.[37] Furthermore, it is also possible that prenatal intra-amniotic injection of Ca^{2+} could prevent or rescue fetal bone abnormalities.

Given that *TRPV6* is expressed in tissues in addition to the placenta, future information could shed light on the role of *TRPV6* in early-onset osteopenia and recurrent fractures of unknown etiology and might illuminate new strategies for preventing Ca^{2+} deficiency in certain types of hyperparathyroidism as well as other conditions associated with a decreased bone mineral density.

In summary, we studied a group of newborns who presented at birth with hyperparathyroidism and clear signs of metabolic bone disease. No apparent cause could be identified, and the bone metabolism normalized within a short time after birth. Genomic analysis revealed biallelic mutations in *TRPV6* in all affected children, and mutation expression studies showed that these mutations strongly interfered with the normal function of *TRPV6*. We thus conclude that interference with the placental maternal-fetal calcium transport caused by *TRPV6* loss-of-function mutations results in fetal calcium deficiency, hyperparathyroidism, and metabolic bone disease. Postnatal recovery or improvement was observed once the maternal-fetal transport of calcium through the placenta ceased and the calcium was being provided orally.

Supplemental Data

Supplemental Data include three figures, a Supplemental Note, and Supplemental Material and Methods and can be found with this article online at https://doi.org/10.1016/j.ajhg.2018.04.006.

Acknowledgments

We thank Matthias A. Hediger (University of Bern, Switzerland) for human TRPV6 cDNA, and we thank Claire T. Saito and Takaaki Sokabe (Okazaki Institute for Integrative Bioscience) for technical assistance and discussion. We also thank the Functional Genomics Facility of the NIBB Core Research Facility for the gel imaging system. This work was supported by a grant-in-aid for scientific research provided to Y.S. and M.T. by the Ministry of Education, Culture, Sports, Science, and Technology (grant number 15K08199) in Japan.

Received: December 25, 2017
Accepted: April 6, 2018
Published: May 31, 2018

Web Resources

GenBank, https://www.ncbi.nlm.nih.gov/genbank/
GeneDx ClinVar submission page, http://www.ncbi.nlm.nih.gov/clinvar/submitters/26957/
ImageJ software, https://imagej.nih.gov/ij/
OMIM, http://www.omim.org

References

1. Salles, J.P. (2016). Bone metabolism during pregnancy. Ann. Endocrinol. (Paris) *77*, 163–168.
2. Tanaka, A.J., Cho, M.T., Millan, F., Juusola, J., Retterer, K., Joshi, C., Niyazov, D., Garnica, A., Gratz, E., Deardorff, M., et al. (2015). Mutations in SPATA5 are associated with microcephaly, intellectual disability, seizures, and hearing loss. Am. J. Hum. Genet. *97*, 457–464.
3. Peng, J.B., Brown, E.M., and Hediger, M.A. (2001). Structural conservation of the genes encoding CaT1, CaT2, and related cation channels. Genomics *76*, 99–109.
4. Fecher-Trost, C., Wissenbach, U., Beck, A., Schalkowsky, P., Stoerger, C., Doerr, J., Dembek, A., Simon-Thomas, M., Weber, A., Wollenberg, P., et al. (2013). The in vivo TRPV6 protein starts at a non-AUG triplet, decoded as methionine, upstream

(B) Representative time trace of whole-cell patch-clamp recordings in HEK293T cells. In the cell expressing WT, monovalent cation current as well as Ca^{2+} current was observed. On the other hand, there were no obvious currents in mock- or p.Arg425Gln-transfected cells when they were incubated with DVF (divalent-cation-free solution) or 30Ca (30 mM Ca^{2+} with NMDG solution). Thin dotted lines indicate zero-current.
Abbreviations are as follows: mock, mock-transfected cell; WT, wild-type TRPV6-transfected cell; p.Arg425Gln, p.Arg425Gln-variant-transfected cell.
(C) Statistical analysis of Ca^{2+} current amplitudes in (B). ($n = 4–6$, $^*p < 0.05$ versus WT, Mann-Whitney test).
(D) Localization of TRPV6 proteins. TRPV6 protein bands (approx. 80 kDa) were observed in WT-, p.Ala18Ser-, or p.Cys212Tyr-transfected cells, but not in p.Ile223Thr-, p.Arg425Gln-, p.Gly428Arg-, p.Gly451Glu-, or p.Arg483Trp-expressing cells.
(E) Immunoblotting of TRPV6 (anti-c-*myc* antibody) with total lysate. The p.Arg425Gln, p.Gly428Arg, and p.Arg483Trp proteins were observed in total lysate, suggesting mislocalization.
(F) Immunoblotting of TRPV6 (anti-c-*myc* antibody) with total lysate from the cells expressing WT or p.Gly451Glu with a shorter time course (24 hr). In this condition, the p.Gly451Glu proteins were detectable (−RuR). When cells with RuR (+RuR) were incubated, the p.Gly451Glu band was more prominent.
RuR, ruthenium red (2 μM).
(G) Measurement of intracellular Ca^{2+} concentration ($[Ca^{2+}]_i$) in a steady state with standard bath solution. The concentration was statistically higher in p.Gly451Glu variant compared to WT ($n = 33–58$, $p < 0.001$ in Mann-Whitney rank-sum test).

of canonical initiation at AUG. J. Biol. Chem. *288*, 16629–16644.
5. Hughes, D.A., Tang, K., Strotmann, R., Schöneberg, T., Prenen, J., Nilius, B., and Stoneking, M. (2008). Parallel selection on TRPV6 in human populations. PLoS ONE *3*, e1686.
6. Zhou, Y., Suzuki, Y., Uchida, K., and Tominaga, M. (2013). Identification of a splice variant of mouse TRPA1 that regulates TRPA1 activity. Nat. Commun. *4*, 2399.
7. Nilius, B., Vennekens, R., Prenen, J., Hoenderop, J.G., Bindels, R.J., and Droogmans, G. (2000). Whole-cell and single channel monovalent cation currents through the novel rabbit epithelial Ca2+ channel ECaC. J. Physiol. *527*, 239–248.
8. Bödding, M., Wissenbach, U., and Flockerzi, V. (2002). The recombinant human TRPV6 channel functions as Ca2+ sensor in human embryonic kidney and rat basophilic leukemia cells. J. Biol. Chem. *277*, 36656–36664.
9. Nilius, B., Weidema, F., Prenen, J., Hoenderop, J.G., Vennekens, R., Hoefs, S., Droogmans, G., and Bindels, R.J. (2003). The carboxyl terminus of the epithelial Ca(2+) channel ECaC1 is involved in Ca(2+)-dependent inactivation. Pflugers Arch. *445*, 584–588.
10. Nilius, B., Prenen, J., Hoenderop, J.G., Vennekens, R., Hoefs, S., Weidema, A.F., Droogmans, G., and Bindels, R.J. (2002). Fast and slow inactivation kinetics of the Ca2+ channels ECaC1 and ECaC2 (TRPV5 and TRPV6). Role of the intracellular loop located between transmembrane segments 2 and 3. J. Biol. Chem. *277*, 30852–30858.
11. Belkacemi, L., Gariépy, G., Mounier, C., Simoneau, L., and Lafond, J. (2004). Calbindin-D9k (CaBP9k) localization and levels of expression in trophoblast cells from human term placenta. Cell Tissue Res. *315*, 107–117.
12. Hacker, A.N., Fung, E.B., and King, J.C. (2012). Role of calcium during pregnancy: maternal and fetal needs. Nutr. Rev. *70*, 397–409.
13. Parkes, I., Schenker, J.G., and Shufaro, Y. (2013). Parathyroid and calcium metabolism disorders during pregnancy. Gynecol. Endocrinol. *29*, 515–519.
14. Pitkin, R.M. (1985). Calcium metabolism in pregnancy and the perinatal period: a review. Am. J. Obstet. Gynecol. *151*, 99–109.
15. Egbuna, O.I., and Brown, E.M. (2008). Hypercalcaemic and hypocalcaemic conditions due to calcium-sensing receptor mutations. Best Pract. Res. Clin. Rheumatol. *22*, 129–148.
16. Lietman, S.A., Tenenbaum-Rakover, Y., Jap, T.S., Yi-Chi, W., De-Ming, Y., Ding, C., Kussiny, N., and Levine, M.A. (2009). A novel loss-of-function mutation, Gln459Arg, of the calcium-sensing receptor gene associated with apparent autosomal recessive inheritance of familial hypocalciuric hypercalcemia. J. Clin. Endocrinol. Metab. *94*, 4372–4379.
17. Nesbit, M.A., Hannan, F.M., Howles, S.A., Reed, A.A., Cranston, T., Thakker, C.E., Gregory, L., Rimmer, A.J., Rust, N., Graham, U., et al. (2013). Mutations in AP2S1 cause familial hypocalciuric hypercalcemia type 3. Nat. Genet. *45*, 93–97.
18. Wagener, B.M., Marjon, N.A., Revankar, C.M., and Prossnitz, E.R. (2009). Adaptor protein-2 interaction with arrestin regulates GPCR recycling and apoptosis. Traffic *10*, 1286–1300.
19. Nesbit, M.A., Hannan, F.M., Howles, S.A., Babinsky, V.N., Head, R.A., Cranston, T., Rust, N., Hobbs, M.R., Heath, H., 3rd, and Thakker, R.V. (2013). Mutations affecting G-protein subunit α11 in hypercalcemia and hypocalcemia. N. Engl. J. Med. *368*, 2476–2486.
20. Li, D., Tian, L., Hou, C., Kim, C.E., Hakonarson, H., and Levine, M.A. (2016). Association of mutations in SLC12A1 encoding the NKCC2 cotransporter with neonatal primary hyperparathyroidism. J. Clin. Endocrinol. Metab. *101*, 2196–2200.
21. Unger, S., Paul, D.A., Nino, M.C., McKay, C.P., Miller, S., Sochett, E., Braverman, N., Clarke, J.T., Cole, D.E., and Superti-Furga, A. (2005). Mucolipidosis II presenting as severe neonatal hyperparathyroidism. Eur. J. Pediatr. *164*, 236–243.
22. Glass, E.J., and Barr, D.G. (1981). Transient neonatal hyperparathyroidism secondary to maternal pseudohypoparathyroidism. Arch. Dis. Child. *56*, 565–568.
23. Lee, B.M., Lee, G.S., Jung, E.M., Choi, K.C., and Jeung, E.B. (2009). Uterine and placental expression of TRPV6 gene is regulated via progesterone receptor- or estrogen receptor-mediated pathways during pregnancy in rodents. Reprod. Biol. Endocrinol. *7*, 49.
24. Bianco, S.D., Peng, J.B., Takanaga, H., Suzuki, Y., Crescenzi, A., Kos, C.H., Zhuang, L., Freeman, M.R., Gouveia, C.H., Wu, J., et al. (2007). Marked disturbance of calcium homeostasis in mice with targeted disruption of the Trpv6 calcium channel gene. J. Bone Miner. Res. *22*, 274–285.
25. Woudenberg-Vrenken, T.E., Lameris, A.L., Weißgerber, P., Olausson, J., Flockerzi, V., Bindels, R.J., Freichel, M., and Hoenderop, J.G. (2012). Functional TRPV6 channels are crucial for transepithelial Ca2+ absorption. Am. J. Physiol. Gastrointest. Liver Physiol. *303*, G879–G885.
26. Peng, J.B., Chen, X.Z., Berger, U.V., Weremowicz, S., Morton, C.C., Vassilev, P.M., Brown, E.M., and Hediger, M.A. (2000). Human calcium transport protein CaT1. Biochem. Biophys. Res. Commun. *278*, 326–332.
27. Weissgerber, P., Kriebs, U., Tsvilovskyy, V., Olausson, J., Kretz, O., Stoerger, C., Vennekens, R., Wissenbach, U., Middendorff, R., Flockerzi, V., and Freichel, M. (2011). Male fertility depends on Ca^2+ absorption by TRPV6 in epididymal epithelia. Sci. Signal. *4*, ra27.
28. Fecher-Trost, C., Wissenbach, U., and Weissgerber, P. (2017). TRPV6: From identification to function. Cell Calcium *67*, 116–122.
29. Wissenbach, U., Niemeyer, B.A., Fixemer, T., Schneidewind, A., Trost, C., Cavalie, A., Reus, K., Meese, E., Bonkhoff, H., and Flockerzi, V. (2001). Expression of CaT-like, a novel calcium-selective channel, correlates with the malignancy of prostate cancer. J. Biol. Chem. *276*, 19461–19468.
30. Peng, J.B., Zhuang, L., Berger, U.V., Adam, R.M., Williams, B.J., Brown, E.M., Hediger, M.A., and Freeman, M.R. (2001). CaT1 expression correlates with tumor grade in prostate cancer. Biochem. Biophys. Res. Commun. *282*, 729–734.
31. Suzuki, Y., Kovacs, C.S., Takanaga, H., Peng, J.B., Landowski, C.P., and Hediger, M.A. (2008). Calcium channel TRPV6 is involved in murine maternal-fetal calcium transport. J. Bone Miner. Res. *23*, 1249–1256.
32. Saotome, K., Singh, A.K., Yelshanskaya, M.V., and Sobolevsky, A.I. (2016). Crystal structure of the epithelial calcium channel TRPV6. Nature *534*, 506–511.
33. Niemeyer, B.A., Bergs, C., Wissenbach, U., Flockerzi, V., and Trost, C. (2001). Competitive regulation of CaT-like-mediated Ca2+ entry by protein kinase C and calmodulin. Proc. Natl. Acad. Sci. USA *98*, 3600–3605.
34. Lambers, T.T., Weidema, A.F., Nilius, B., Hoenderop, J.G., and Bindels, R.J. (2004). Regulation of the mouse epithelial Ca2(+)

channel TRPV6 by the Ca(2+)-sensor calmodulin. J. Biol. Chem. *279*, 28855–28861.

35. Hoenderop, J.G., Vennekens, R., Müller, D., Prenen, J., Droogmans, G., Bindels, R.J., and Nilius, B. (2001). Function and expression of the epithelial Ca(2+) channel family: comparison of mammalian ECaC1 and 2. J. Physiol. *537*, 747–761.
36. Phelps, C.B., Huang, R.J., Lishko, P.V., Wang, R.R., and Gaudet, R. (2008). Structural analyses of the ankyrin repeat domain of TRPV6 and related TRPV ion channels. Biochemistry *47*, 2476–2484.
37. Bosch, B., and De Boeck, K. (2016). Searching for a cure for cystic fibrosis. A 25-year quest in a nutshell. Eur. J. Pediatr. *175*, 1–8.